Adhesion layer-bottom electrode interaction during BaxSr1−xTiO3 growth as a limiting factor for device performance

Markus Löffler, Andrei Vorobiev, Lunjie Zeng, Spartak Gevorgian, and Eva Olsson

Related Articles

Additional information on J. Appl. Phys.

Adhesion layer-bottom electrode interaction during $Ba_xSr_{1-x}TiO_3$ growth as a limiting factor for device performance

Markus Löffler,[1] Andrei Vorobiev,[2] Lunjie Zeng,[1] Spartak Gevorgian,[2] and Eva Olsson[1]

[1]*Department of Applied Physics, Chalmers University of Technology, Gothenburg SE-41296, Sweden*
[2]*Department of Microtechnology and Nanoscience, Chalmers University of Technology, Gothenburg SE-41296, Sweden*

Changes in bottom electrode morphology and adhesion layer composition upon deposition of $Ba_xSr_{1-x}TiO_3$ (BSTO) at elevated temperatures have been found, which have a negative impact on acoustic wave resonator device performance. The difference between nominal and actual adhesion layer composition are explained by grain boundary diffusion of Ti or W and their oxidation by in-diffusing oxygen, which leads to an increased interface roughness between the Pt bottom electrode and the BSTO. It is shown, that room-temperature deposited TiO_2 diffusion barriers fail to protect against Ti oxidation and diffusion. Also W adhesion layers are prone to this phenomenon, which limits their ability to act as high temperature resistant adhesion layers for bottom electrodes for ferroelectric thin films. © *2012 American Institute of Physics*. [http://dx.doi.org/10.1063/1.4730781]

I. INTRODUCTION

One of the prerequisites on the road to new, tunable ferroelectric materials is the reliability and consistency of the underlying electrode structures under the growth conditions of the respective thin films. Especially roughness has to be controlled to reduce acoustic scattering, e.g., in $Ba_xSr_{1-x}TiO_3$ (BSTO) thin film bulk acoustic resonators (FBARs). Scattering of waves and a broadening of the resonance frequency due to local thickness variations are two examples of loss mechanisms associated with rough interfaces.[1,2] In contrast to non-tunable AlN FBARs operating below 2 GHz, where the typical interface roughness is far below the acoustical wavelength,[1,3] for BSTO devices operating at 5.2 GHz, these kinds of losses cannot be neglected. This is mainly a consequence of the higher operating frequency as well as the significantly lower BSTO sound velocity. The corresponding reduction in the acoustical wavelength by about a factor 4 places significantly higher demands on interface smoothness in BSTO based resonator devices. Scattering at interfaces with a root-mean-squared roughness even less than 10 nm has been shown to have severe impact on the device performance.[4] Furthermore, the electrode material should possess a large work function to suppress charge injection and leakage currents and ohmic losses in the electrodes should be as small as possible. One electrode material which fulfills these prerequisites is Pt, mainly due to its resistance to oxidation and its high electrical conductivity[5] as well as its high Schottky barrier.[6] However, Pt adheres poorly to SiO_2, which hinders the successful implementation of these devices into Si-based electronics. Combinations of an adhesion layer (mainly Ti) and possibly a diffusion barrier have been suggested in the past in the search for suitable electrodes for PZT $(Pb[Zr_xTi_{1x}]O_3)$.[5,7,8]

In this paper, we present the results of microstructural investigations of the influence of the interfacial interaction between the adhesion layer, diffusion barrier, and Pt bottom electrode during BSTO growth. The growth temperature is a key parameter for the BSTO acoustic performance. Therefore, adhesion layer, diffusion barrier, and bottom electrode

material have to withstand the high temperature as well as the oxygen containing atmosphere during BSTO deposition and annealing. Morphological changes in the bottom electrode and adhesion layer as well as changes in composition have been observed. The information is invaluable for further improvement of the Q-factor by optimization of the choice of materials and process parameters for BSTO based devices.

II. EXPERIMENTAL

Two samples were selected for microstructural investigation based on their acoustic performance. One sample, with the BSTO film grown at 585 °C, showed the best performance (highest Q-factor)[9] while the other sample showed a strongly degraded performance, although it was grown at higher temperature (625 °C) which favors the higher crystallinity of the BSTO film.

The samples were prepared by magnetron sputtering with 500 W rf power (radiofrequency, 1.76 MHz) and at different BSTO deposition temperatures. A multilayer consisting of three layers of SiO_2 and two layers of W were deposited at room temperature on a 6 in. Si wafer with nominal thicknesses of 240 nm and 280 nm, respectively. The absolute values of these film thicknesses were expected to vary slightly with distance from the center along the radius of the 4 in. wafer. These layers constitute the so-called Bragg reflector, which provides acoustic isolation of the resonator from the substrate. To improve adhesion between the top a-SiO_2 layer and the Pt bottom electrode, an adhesion layer and in the case of the 625 °C sample an additional diffusion barrier were employed. The sample with the BSTO film grown at 585 °C featured a nominal W layer and the 625 °C sample a nominal Ti/TiO_2 bilayer due to issues with delamination when using W at higher temperatures. A 100 nm Pt layer, serving as the bottom electrode for the BSTO, was sputtered at room temperature directly afterwards. For BSTO film deposition, the sample was slowly brought up to deposition temperature by backside irradiation in an 8 mTorr Ar/O_2

1:1 atmosphere. BSTO films with a nominal thickness of 290 nm were sputtered in on-axis geometry (10 cm target-substrate distance) from a stoichiometric target at different substrate temperatures at 2 mTorr Ar/O$_2$ 1:1 atmosphere. The sample was left to cool down in 600 Torr O$_2$ atmosphere. A patterned Al layer with 100 nm thickness served as top electrode. The above conditions were chosen in order to achieve a good film texture (111). This means, that the columnar grains show as little misalignment with respect to the surface normal as possible and that their mean tilt angle is close to zero. This is necessary in order to reduce the generation of shear waves by grain boundaries or inclined grains with respect to the electrodes,[10,11] a phenomenon which is known from AlN-based devices. Especially, a low deposition pressure is required to prevent a thermalization of the sputtered species. It has been shown that films deposited with non-thermalized species show a better texture and crystalline quality due to increased surface mobility and overall higher impact energy.[12] The target-substrate distance was therefore chosen to be smaller than their mean-free path. Further details concerning the design and fabrication of the FBAR test structures can be found in Ref. 13.

The samples were studied by transmission electron microscopy (TEM) using a Tecnai G2 ST 200 kV LaB$_6$ TEM with a high angle annular dark field scanning TEM (HAADF STEM) detector. Thin lamellae for TEM investigations were prepared by the focused ion beam (FIB) liftout technique using 30 kV Ga ions in a Fei Strata DB235 Dual Beam instrument. The final thinning was performed using an incidence angle of 1°–2° at 5 kV and 100 nA Ga ion beam. Additional fine polishing was made using 3 mA low kV (0.7 kV to 1 kV) Ar ions in a Fischione Model 1010 Low Angle Ion Milling and Polishing System. The samples were analyzed with respect to roughness of the bottom electrode, roughness of the BSTO surface, and morphologies at the different interfaces. Energy electron loss spectroscopy (EELS) was performed using a probe C$_s$-corrected Titan 80–300 TEM/STEM. Energy dispersive x-ray spectroscopy (EDX) was performed on both the Titan and Tecnai microscopes.

The roughness of the interface between the bottom Pt electrode and BSTO was quantified using a reference line parallel to the substrate surface. The distance between the reference line and the Pt/BSTO interface was measured every 30 nm. This sampling was fine enough to capture height changes in the bottom electrode. A total of about 1 μm per micrograph was used for calculation of the roughness values where the mean y_0 and corresponding S_q (root-mean-squared roughness) values were extracted with the following equation:

$$S_q = \sqrt{\frac{1}{N} \sum_{i=1}^{N} (y_i - y_0)^2},$$

where N is the number of points in each micrograph and y_i is the height above a line parallel to the substrate. Finally, all S_q values were averaged over all available micrographs.

The electroacoustic properties of these samples were determined by capacitance measurements at 1.0 MHz and by complex impedance measurements in the frequency range up to 10 GHz using a vector network analyzer. Subsequently, the modified Butterworth-Van Dyke model and a de-embedding procedure were used to calculate the series resistances of the electrodes and acoustic parameters of the BSTO film. Details on the electroacoustic properties and their measurement can be found in Ref. 9. The sheet resistance of the Pt bottom electrode was both measured on a Pt/TiO$_2$ sample as well as on a Pt/W sample annealed using the parameters of the BSTO film deposition. With a value of about 3.6 Ω in both cases, it is significantly larger than the bulk counterpart value of 1.06 Ω.[9]

III. RESULTS

An overview over the sample properties is presented in Table I, which includes the acoustic Q-factor as well as the roughness for the top and bottom interface of the BSTO layer measured by AFM and TEM, respectively. The sample grown at 585 °C showed the highest Q-factor in our growth series. We found that the Q-factor of the devices increased with growth temperature due to a reduction in the amorphous layer between the bottom electrode and the BSTO-layer, a reduction of oxygen vacancies and BSTO(111) texture misalignment.[9] However, a strong drop in Q-factor for growth temperatures above 590 °C was observed. This decrease can be attributed to a sharp increase in roughness resulting in generation of shear waves and resonance broadening by local thickness variations.[9] The origin of that phenomenon can be traced back to changes in the bottom electron/adhesion layer microstructure during high temperature deposition of BSTO and will be discussed later on.

A. Bragg reflector

The overall structure of the multilayers can be seen in the TEM micrograph presented in Fig. 1. The lower part is a Si substrate on top of which there are three layers of amorphous SiO$_2$ and two layers of polycrystalline W (as determined from high-res TEM, not shown) in an alternating sequence forming the Bragg reflector for acoustic waves, as described in Sec. II. XRD showed that the SiO$_2$ layers were partially crystallized in the 585 °C sample (for details see Ref. 9). On the other hand, the TEM showed that the SiO$_2$ layers were amorphous. No crystalline regions were observed in either of the specimens. Since electron diffraction can be obtained from smaller crystalline volumes compared to x-ray diffraction and that TEM provides local information and the x-rays an average information, the difference between the two methods may be due to the presence

TABLE I. Properties of the samples and the respective BSTO growth temperatures.

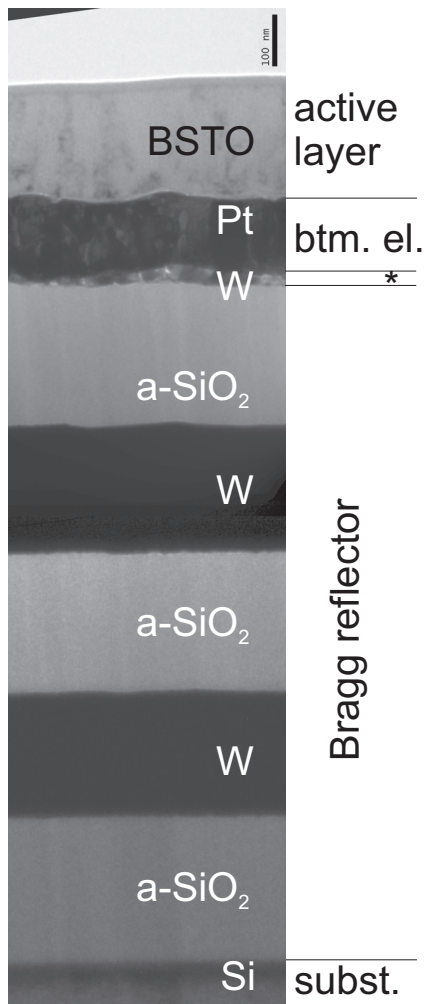| T_g (°C)	Acoustic Q-factor	Adhesion layer	Pt layer roughness S_q (nm)	BSTO top surface roughness S_q (nm)
585	355	W	14	3.5
625	185	Ti/TiO$_2$	39	6

FIG. 1. TEM cross section (stitched micrographs): Overview over the sample structure based on the sample grown at 585 °C. The top Al layer has been removed. The layer denoted by * is the adhesion layer.
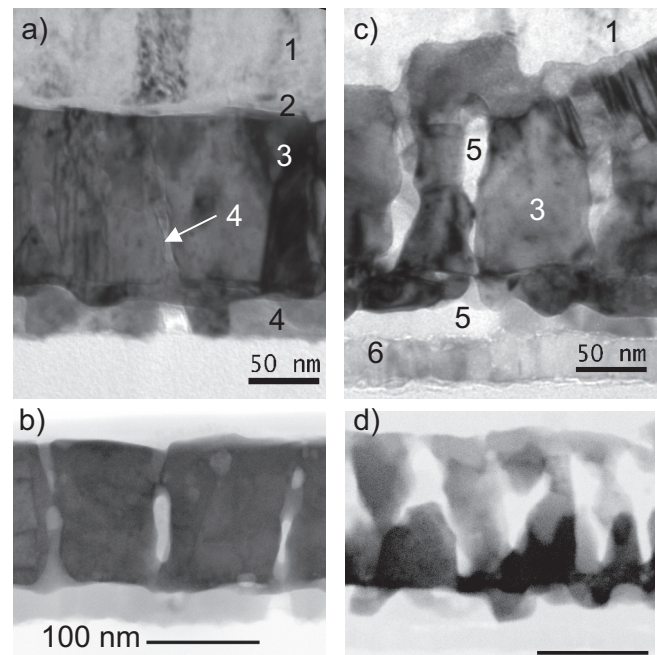

FIG. 2. Bright field (a) and (c) and inverted HAADF (b) and (d) micrographs of the bottom electrode region for the two samples grown at 585 °C (a) and (b) and 625 °C (c) and (d). The bright areas in the HAADF images are indicative of low-Z compounds compared to Pt. The numbers indicate 1 – BSTO, 2 – amorphous layer, 3 – Pt, 4 – WO_x, 5 – TiO_x from nominal TiO_2 layer, 6 – TiO_x from nominal Ti layer. Scale bars in (b) and (d) are of the same size.

of a low percentage of highly localized crystalline SiO_2 in the 585 °C and possibly also the 625 °C sample.

B. Adhesion layer/bottom electrode morphology and composition

The interfaces between the SiO_2 and the adhesion layers are flat interfaces in both cases (see Fig. 2). The same is valid for the interface between the Pt and the adhesion layer for the 585 °C sample (Figs. 2(a) and 2(b)). The high temperature sample (Figs. 2(c) and 2(d)) shows a reduced thickness of the TiO_2 layer and oxidation of the Ti layer. Occasionally, small voids are observed between the oxidized Ti and SiO_2 layers, but of much more interest is the interaction between the top TiO_2 and the Pt layer.

EELS and EDX investigations showed the presence of oxygen in the adhesion layers and diffusion barriers of all samples. In the samples grown at 585 °C, Figs. 2(a) and 2(b), and 625 °C, Figs. 2(c) and 2(d), WO_x and TiO_x, respectively, are also observed inside the Pt layer. The oxides are mainly present in the Pt grain boundary regions and the effect is much more pronounced in the 625 °C sample. The difference between the 585 °C and 625 °C samples can be attributed

both to the higher melting point of W compared to Ti and the overall lower process temperature.

In detail, the 625 °C sample, with a nominal Ti/TiO_2 bilayer, showed oxidation of Ti to TiO_x. Furthermore, TiO_2 was found to be present in the Pt bottom electrode (Fig. 3, upper panels) as a comparison of low-loss EELS spectra obtained from the inclusion in the electrode with standard (bulk) TiO_2 spectra shows. It can be expected that the prolonged exposure to the high temperatures during BSTO deposition (ramp up/deposition/cool down) and diffusing oxygen led to an oxidation of the Ti film.

In the nominal W layer, in the 585 °C sample, oxygen was evenly distributed in the layer giving rise to a tungsten oxide layer (see Fig. 3, lower panels). This oxide was also found in the Pt layer at Pt grain boundaries, Figs. 2(c) and 2(d). The oxygen core loss peak (O_K) fine structure varies from inclusion to inclusion, a behavior known to stem for the different polytypes of WO_3.[14] The low-loss EELS data indicate incomplete oxidation both of the W layer as well as the inclusions in the Pt layer. In detail, both the layer and the inclusion show O_K peaks and W_M peaks. The EELS low-loss data (Fig. 3, lower right panel) contains both transitions from W5p1/2 and W5s to unoccupied states at 43 eV and 54 eV, respectively.[15,16] The broad peak at approximately 24 eV is common to both W and WO_3 and can be attributed to the W bulk plasmon[12] and/or an O2s to W5d transition at slightly lower energy.[16,17] However, the peak at 14 eV and the shoulder around 6 eV only occur in oxidized W[15–17] and are attributed to O2p to W5d and W6s or W5f transitions in WO_3, respectively.[17,18] Overall, the material can best be described as WO_x with x approximately 1, as a comparison
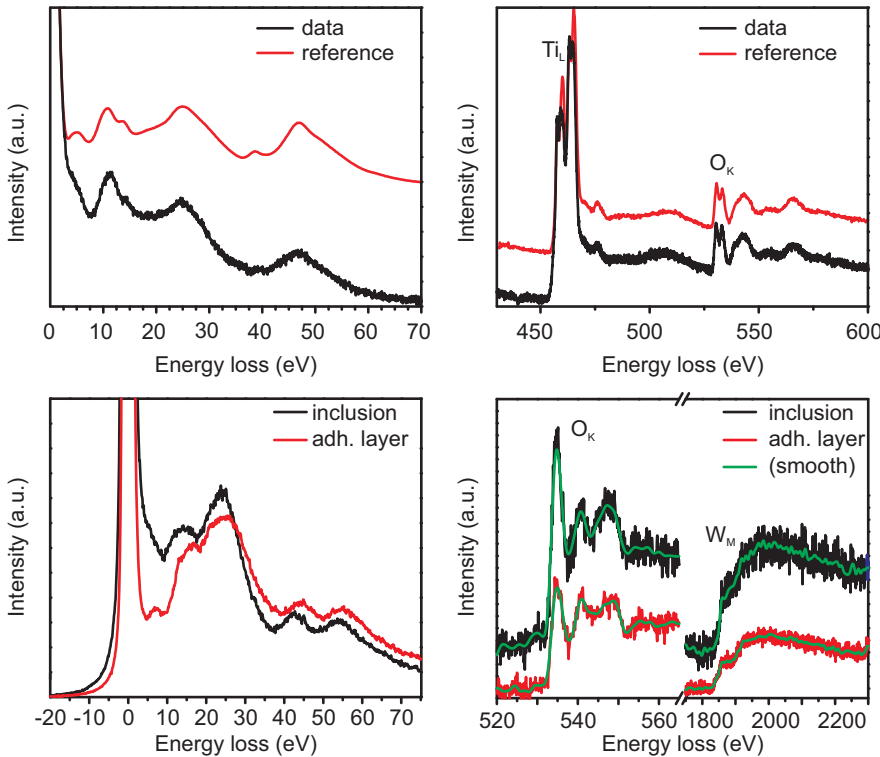
FIG. 3. Low loss (left) and core loss (right) EELS spectra taken on the TiO_2 (upper panels) and WO_x (lower panels) inclusions in the Pt bottom electrode. The spectra of WO_x also show a comparison with the adhesion layer.

of low-loss EELS data with literature shows.[15,19] It should be noted, that the latter peaks shift slightly to higher energies (16 eV and 7 eV, respectively) for the adhesion layer compared to the inclusions in the Pt layer (Fig. 3). The reason for this is not entirely clear. The shoulder at 6 eV is rather broad for an interband transition in the inclusion, which can be related to size effects and charge transfer from the surrounding Pt. While it is sharper in the adhesion layer, it is also reduced in intensity hinting at a more metallic character of this film.[17] On the other hand, the 24 eV peak is broader in the adhesion layer, which indicates a more even mixture of O2s and W bulk plasmon contributions. Taking into account the diffusion path of oxygen through the platinum layer, one can safely assume that the oxidation state of the adhesion layer is less than for the inclusions. The cause for the small shift in energy for the W5p1/2 peak cannot be clearly determined. All the peaks depend sensitively on the amount of charge carriers in the conduction bands.[15,16] Since also the intensity of the O1s to W5d transition (lowest-energy peak of the O_K core-loss, Fig. 3) decreases compared to the inclusion, this can be linked to charge injection into a conduction band, which has contributions of W5d and O2p states.[16]

IV. DISCUSSION

The following discussion will focus on the 625 °C sample and the mechanism involving the Pt/TiO_2 phase intermixing. This seems to be the main cause of device performance degradation due to increased series resistance and scattering of acoustic waves by rough top and bottom electrodes.[4] However, the same arguments can also be applied to the 585 °C sample and Pt/WO_x phase intermixing, keeping the lower deposition temperature and lower diffusion coefficient of W in mind. For the sake of simplicity, the adhesion layer and diffusion barrier in the 625 °C sample are only referenced as adhesion layers, since both were found to be TiO_x.

Plastic deformation of Pt films on Ti including void generation and island formation have been observed in annealing experiments[5,7,20–23] at temperatures as low as 450 °C.[21] Annealing of Pt/Ti bilayer metallizations in O containing atmosphere and at elevated temperatures allows for O and Ti diffusion and their reaction to TiO_x which also happens in the Pt layer.[7,8,24,25] This kind of phase intermixing due to diffusion of Ti and reaction with O in Pt grain boundaries has been reported before.[8,21,26] The resulting TiO_x expands in volume by a factor of 1.8,[21] which generates strong compressive stresses that deform and push the Pt grains towards the interfaces on each side. This explains the presence of TiO_2-filled voids and the Pt hillocks on either side of the film. It should be mentioned that grain boundary diffusion of oxygen has even been observed at room temperature,[27] while Ti diffusion was found to be significantly enhanced for temperatures above 600 °C.[20,25] In our system, the heating to the BSTO deposition temperature takes 60 min in 8 mTorr Ar/O₂ atmosphere. The deposition time of the BSTO is 75 min at 2 mTorr Ar/O₂ and the cool down period is about 60 min long and takes place under 600 Torr O₂ atmosphere. Assuming the diffusion constants of $D_{O,900K} = 10^{-7} cm^2/s$ and $D_{Ti,900K} = 10^{-13} cm^2/s$ (Refs. [28] and [29]) and a rough estimate of an exposure to the elevated temperatures around 900 K for about $t = 100$ min, we can estimate the diffusion length $2\sqrt{Dt}$ to about 500 μm for oxygen and 0.5 μm for titanium. With a Pt film thickness of only 100 nm, this is more than enough to explain the observed effects. It should be noted that oxygen might already be present at the Pt grain boundaries. Oxygen in Pt grain boundaries is suspected to be the main reason for reduced electrical conductivity in Pt[20]

deposited in oxygen containing atmospheres including residual oxygen after oxygen containing sputter processes such as TiO_2 in our case. It has also been observed that oxygen favors island formation in Ti/Pt films by amplifying agglomeration of Pt.[23] The individual laterally extended and flat Pt grains that are visible in Fig. 2 hint towards the interaction of growing BSTO and Pt layer reorganization. Similar effects have been observed in PZT films on Pt.[7] These experiments showed that the PZT reduces thermal grooving but reproduces the rough Pt bottom layer, although with reduced amplitude a feature which is also observed in our BSTO samples.

Sreenivas and Al-Shareef found that TiO_2 diffusion barriers between Ti and Pt reduce Pt layer roughnesses and improve adhesion.[7,8] However, we found that the nominal Ti layer in the 625 °C sample converted to TiO_x, as evidenced by EDX analysis. The failure of the nominal TiO_2 layer to protect against Ti and O diffusion can most likely be attributed to the film growth conditions. In contrast to the Refs. 7 and 8, our films were sputter deposited at room temperature in an oxygen-containing atmosphere. Such conditions lead to an amorphous TiO_x film.[30,31] These suboxides do not offer good protection against Ti and most likely also O diffusion.[8,32] It can be assumed that our sputtered TiO_2 is not stoichiometric, allowing diffusion of Ti into Pt grain boundaries and oxidation forming TiO_2 (as evidenced by EELS analysis, see Fig. 3, upper panels). In-diffusing oxygen would oxidize the remaining Ti.[33]

As evidenced by EDX and EELS (Fig. 3, lower panels), the diffusion of W and O also takes places in a similar manner at 585 °C. Small inclusions of WO_x in Pt grain boundaries show that also W diffuses, similar to Ti, albeit at a much slower speed due to the higher melting point of W and the lower processing temperatures.

Although the O diffusion should also be slower due to the dependence of the diffusion coefficient on temperature, the processing time is long enough for oxygen to reach the 20 nm W layer. However, the presence of WO_3 could not be determined unambiguously. EELS data from the O_K absorption edge of WO_3 has been shown to depend on the environment and coordination of O and vary with the polytype.[14] Furthermore, literature data[15] for the low-loss region indicate only weak oxidation of W in spectra from our studies. The best description of the layer would be WO_x, where x is approximately 1. There are some differences between the WO_x, which is incorporated into the Pt grain boundaries and the one in the adhesion layer. The adhesion layer is in general less oxidized compared to the inclusions. It cannot be clearly distinguished if the overall stoichiometry of WO_x with x approximately equal to 1 stems from a homogeneous distribution of oxygen or of WO_3 clusters embedded in a W or W_3O matrix.[19]

The observed voids in the adhesion layer from diffusion of W and the inclusion of WO_x into Pt grain boundaries are not beneficial to overall device performance. They result in a loss of adhesion, and WO_x inclusion in the Pt layer reduces the quality of the bottom electrode. Therefore, W is not suitable as an adhesion layer for ferroelectric ceramics due to the presence of oxygen during growth and post-deposition annealing.

The higher sheet resistance of the Pt bottom electrode annealed using the BSTO deposition conditions can most likely be attributed to the oxidation of Pt (Ref. 9) and the formation of TiO_2 inclusions.[9] However, it should be noted that the impact of sheet resistance on the measured series resistance is small, as the main contribution to the series resistance stems from the contact resistance between the probe tips and the top electrode.[9]

V. CONCLUSION

Results of microstructural investigations on the effect of interface morphology and composition of sputtered bottom electrode metallizations were presented. A deformation of the Pt bottom electrode has been found, which is closely linked to changes in the adhesion layer and diffusion barrier microstructure and composition. It has been found that room temperature deposited TiO_2 layers fail as a diffusion barrier due to their amorphous and probably non-stoichiometric nature. The diffusion of adhesion layer and diffusion barrier atoms and oxygen along the Pt grain boundaries results in inclusions of their respective oxides. These oxides expand upon formation, which results in a force that pushes Pt grains towards the layer interfaces and induces hillocking of the Pt film. Even in the case of a high melting point, material such as W diffusion has been observed and the nominal W film was found to be slightly oxidized to WO_x ($x \approx 1$). The diffusion of adhesion layer atoms and subsequent oxidation cause a reduced conductivity and an increase in roughness of the bottom electrode. While the former increases the ohmic losses, the latter results in the undesired scattering of acoustic waves and the generation of shear waves, which in turn may leak through the Bragg reflector.[1] Both increases in sheet resistance by oxide inclusions and degraded acoustic properties lead to a reduced device performance. To date, similar BSTO-based resonator devices are disappointing due to low Qf-products, most often in the range of 400–750 GHz.[34–36] Although our devices show the highest Q-factors, or more precisely, the highest Qf-product of more than 1300 GHz,[13] there is still room for improvement. Our findings can help to improve the performance by setting a clear frame on the device design and growth conditions by taking into account the dynamic nature of adhesion layer/bottom electrode interaction.

[1]K.-Y. Hashimoto, *RF Bulk Acoustic Wave Filters for Communications* (Artech House, Norwood, MA, 2009).
[2]J. Berge, A. Vorobiev, W. Steichen, and S. Gevorgian, IEEE Microw. Wirel. Componen. Lett. **17**, 655 (2007).
[3]R. Thalhammer, J. Kaitila, R. Aigner, and S. Marksteiner, Proc.–IEEE Ultrason. Symp. **1**, 282 (2004).
[4]A. Vorobiev, J. Berge, S. Gevorgian, M. Löffler, and E. Olsson, J. Appl. Phys. **110**, 024116 (2011).

[5]L. D. Madsen, L. Weaver, H. Ljungcrantz, and A. J Clark, J. Electron. Mater. **27**, 418 (1998).

[6]T.-S. Chen, V. Balu, S. katakam, J.-H. Lee, and C. Lee, IEEE Trans. Electron Devices **46**(12), 2304 (1999).

[7]H. N. Al-Shareef, D. Dimos, and B. A. Tuttle, J. Mater. Res. **12**, 347 (1997).

[8]K. Sreenivas, I. Reaney, T. Maeder, N. Setter, C. Jagadish, and R. G. Elliman, J. Appl. Phys. **75**, 232 (1994).

[9]A. Vorobiev, S. Gevorgian, M. Löffler, and E. Olsson, J. Appl. Phys. **110**, 054102 (2011).

[10]F. Martin, M.-E. Jan, B. Belgacem, M.-A. Dubois, and P. Muralt, Thin Solid Films **514**, 341 (2006).

[11]J. Bjurström, G. Wingqvist, and I. Katardjiev, Proc.–IEEE Ultrason. Symp. **2005**, 321.

[12]G. F. Iriarte, F. Engelmark, and I. V. Katardjiev, J. Mater. Res. **17**, 1469 (2002).

[13]A. Vorobiev and S. Gevorgian, Appl. Phys. Lett. **92**, 212904 (2010).

[14]M. R. Field, D. G. McCulloch, S. N. H. Lim, A. Anders, V. J. Keast, and R. W Burgess, J. Phys.: Condens. Matter **20**, 175216 (2008).

[15]G. Soto, W. De La Cruz, J. A. Díaz, R. Machorro, F. F. Castillón, and M. H. Farías, Appl. Surf. Sci. **218**, 281 (2003).

[16]S. Hashimoto and H. Matsuoka, J. Appl. Phys. **69**, 933 (1991).

[17]M. Gillet, K. Aguir, C. Lemire, E. Gillet, and K. Schierbaum, Thin Solid Films **467**, 239 (2004).

[18]J. J. Ritsko, H. Witzke, and S. K. Deb, Solid State Commun. **22**, 455 (1977).

[19]Y. G. Shen, Y. W. Mai, W. E. McBride, D. R. McKenzie, and Q. C. Zhang, Appl. Phys. Lett. **75**, 2211 (1999).

[20]U. Schmid, J. Appl. Phys. **103**, 054902 (2008).

[21]W. Hartner, Ph.D. dissertation, RWTH Aachen, 2003.

[22]K. Nakamura, Y. Otani, M. Kurita, S. Okamura, and T. Shiosaki, Jpn. J Appl. Phys., Part 1 **44**, 8096 (2005).

[23]S. L. Firebaugh, K. F. Jensen, and M. A. Schmidt, J. Microelectromech. Syst. **7**, 128 (1998).

[24]M. Aspelmeyer, U. Klemradt, W. Hartner, H. Bachhofer, and G. Schindler, J. Phys. D **34**, A173 (2001).

[25]J. O. Olowafe, R. E. Jones, A. C. Campbell, R. I. Hedge, C. J. Mogab, and R. B. Gregory, J. Appl. Phys. **73**, 1764 (1993).

[26]V. Gurumurthy, M.Sc. thesis, University of South Florida, 2007.

[27]R. Schmiedl, V. Demuth, P. Lahnor, H. Godehardt, Y. Bodschwinna, C. Harder, L. Hammer, H.-P. Strunk, M. Schulz, and K. Heinz, Appl. Phys. A **62**, 223 (1996).

[28]R. Stumpf, C.-L. Liu, and C. Tracy, Phys. Rev. B **59**, 16047 (1999)

[29]M. DiBattista and J. W. Schwank, J. Appl. Phys. **86**, 4902 (1999).

[30]W. S. Lin, L. M. Kao, W. P. Li, C. Y. Hsu, and K. H. Hou, J. Mater. Eng. Perform. **20**, 1063 (2011).

[31]C. H. Heo, S.-B. Lee, and J.-H. Boo, Thin Solid Films **475**, 183 (2005).

[32]Y. Xu and M. R. Shen, Appl. Phys. A **94**, 275 (2009).

[33]T.-N. Lin, J. P. Chu, S.-F. Wang, and C. H. Wu, Jpn. J. Appl. Phys., Part 1 **44**, 5049 (2005).

[34]A. Noeth, T. Yamada, P. Muralt, A. K. Tagantsev, and N. Setter, IEEE T. Ultrason. Ferr., **57**, 379 (2010).

[35]J. Berge and S. Gevorgian, IEEE Trans. Ultrason. Ferroelectr. Freq. Control **58**, 2768 (2011).

[36]G. N. Saddik, D. S. Boesch, S. Stemmer, and R. A. Zork, IEEE MTT-S Int. Microwave Symp. Dig. **2008**, 1263.